Research Square

Preprints are preliminary reports that have not undergone peer review.
They should not be considered conclusive, used to inform clinical practice,
or referenced by the media as validated information.

Longitudinal systemic and medullary immune profiling identifies candidate immune mediator signatures associated with mortality in pediatric B-cell acute lymphoblastic leukemia

Fábio Magalhães-Gama
Fundação Oswaldo Cruz Centro de Pesquisas René Rachou: Fundacao Oswaldo Cruz Instituto Rene Rachou

Flavio Souza Silva
Federal University of Amazonas: Universidade Federal do Amazonas

Mateus Souza Barros
Federal University of Amazonas: Universidade Federal do Amazonas

Izabela Cabral Freitas
University of Amazonas State: Universidade do Estado do Amazonas

Júlia Santos Moraes
Federal University of Amazonas: Universidade Federal do Amazonas

Juliana Costa Ferreira Neves
University of Amazonas State: Universidade do Estado do Amazonas

Claudio Lucas Santos Catão
Federal University of Amazonas: Universidade Federal do Amazonas

Julia Goes Souza Ghedini
Fundação Hospitalar de Hematologia e Hemoterapia do Amazonas: Fundacao Hospitalar de Hematologia e Hemoterapia do Amazonas

Nilberto Dias Araújo
Fundação Hospitalar de Hematologia e Hemoterapia do Amazonas: Fundacao Hospitalar de Hematologia e Hemoterapia do Amazonas

Fabíola Silva Alves-Hanna
Fundação Hospitalar de Hematologia e Hemoterapia do Amazonas: Fundacao Hospitalar de Hematologia e Hemoterapia do Amazonas

Dayane Andriotti Otta
Oswaldo Cruz Foundation Rene Rachou Institute: Fundacao Oswaldo Cruz Instituto Rene Rachou

Ana Carolina Campi-Azevedo
Oswaldo Cruz Foundation Rene Rachou Institute: Fundacao Oswaldo Cruz Instituto Rene Rachou

Ismael Artur Costa-Rocha
Oswaldo Cruz Foundation Rene Rachou Institute: Fundacao Oswaldo Cruz Instituto Rene Rachou

Gabriel Rocha Fernandes
Oswaldo Cruz Foundation Rene Rachou Institute: Fundacao Oswaldo Cruz Instituto Rene Rachou
Gemilson Soares Pontes
Instituto Nacional de Pesquisas da Amazonia
Maria Perpétuo Socorro Sampaio Carvalho
Fundação Hospitalar de Hematologia e Hemoterapia do Amazonas: Fundacao Hospitalar de Hematologia e Hemoterapia do Amazonas
Andréa Monteiro Tarragô
Fundação Hospitalar de Hematologia e Hemoterapia do Amazonas: Fundacao Hospitalar de Hematologia e Hemoterapia do Amazonas
Adriana Malheiro
Federal University of Amazonas: Universidade Federal do Amazonas
Olindo Assis Martins-Filho
Oswaldo Cruz Foundation Rene Rachou Institute: Fundacao Oswaldo Cruz Instituto Rene Rachou
Allyson Guimarães Costa
allyson.gui.costa@gmail.com
Federal University of Amazonas: Universidade Federal do Amazonas https://orcid.org/0000-0002-7312-6822
Andréa Texeira-Carvalho
Oswaldo Cruz Foundation Rene Rachou Institute: Fundacao Oswaldo Cruz Instituto Rene Rachou

---

Research Article

Keywords: B-cell acute lymphoblastic leukemia, tumor microenvironment, immune signatures, immune biomarkers, risk stratification

Posted Date: August 13th, 2026

DOI: https://doi.org/10.21203/rs.3.rs-10540398/v1

License: This work is licensed under a Creative Commons Attribution 4.0 International License.
Read Full License

Longitudinal systemic and medullary immune profiling identifies candidate immune mediator signatures associated with mortality in pediatric B-cell acute lymphoblastic leukemia

Fábio Magalhães-Gama[1,2,3]; Flavio Souza Silva[1,4]; Mateus Souza Barros[1,4]; Izabela Cabral Freitas[1,5]; Júlia Santos Moraes[1,4]; Juliana Costa Ferreira Neves[1,6]; Claudio Lucas Santos Catão[1,4]; Julia Goes Souza Ghedini[1]; Nilberto Dias Araújo[1]; Fabíola Silva Alves-Hanna[1]; Dayane Andriotti Otta[2]; Ana Carolina Campi-Azevedo[2]; Ismael Artur Costa-Rocha[2]; Gabriel Rocha Fernandes[3,7]; Gemilson Soares Pontes[1,8]; Maria do Perpétuo Socorro Sampaio Carvalho[1]; Andréa Monteiro Tarragô[1,4,5]; Adriana Malheiro[1,4,5]; Olindo Assis Martins-Filho[2,3,5]; Allyson Guimarães Costa[1,4,5‡*] & Andréa Texeira-Carvalho[2,3,5‡*]

[1]Fundação Hospitalar de Hematologia e Hemoterapia do Amazonas (HEMOAM), Diretoria de Ensino e Pesquisa, Manaus, Brazil;

[2]Instituto René Rachou - Fundação Oswaldo Cruz (FIOCRUZ-Minas), Grupo Integrado de Pesquisas em Biomarcadores, Belo Horizonte, Brazil;

[3]Instituto René Rachou - Fundação Oswaldo Cruz (FIOCRUZ-Minas), Programa de Pós-graduação em Ciências da Saúde, Belo Horizonte, Brazil;

[4]Universidade Federal do Amazonas (UFAM), Programa de Pós-graduação em Imunologia Básica e Aplicada, Manaus, Brazil;

[5]Universidade do Estado do Amazonas, Programa de Pós-graduação em Ciências Aplicadas à Hematologia, (UEA), Manaus, Brazil;

[6]Universidade do Estado do Amazonas (UEA), Programa de Pós-graduação em Medicina Tropical, Manaus, Brazil;

[7]Instituto René Rachou - Fundação Oswaldo Cruz (FIOCRUZ-Minas), Grupo de Diagnóstico e Terapia de Doenças Infecciosas e Câncer, Belo Horizonte, Brazil;

[8]Instituto Nacional de Pesquisas da Amazônia (INPA), Laboratório de Virologia e Imunologia, Manaus, Brazil.

[‡]These authors share senior authorship

Corresponding Authors:

Allyson Guimarães da Costa - allyson.gui.costa@gmail.com, UFAM, Av. Rodrigo Otávio Jordão Ramos, 1200, Coroado, Manaus, AM, CEP 69067-005, Brazil;

Andréa Texeira-Carvalho - atcteixeira@gmail.com, Instituto René Rachou – FIOCRUZ-Minas, Av. Augusto de Lima, 1715, sala 115, Belo Horizonte, MG, CEP: 30.190-009, Brazil.

ABSTRACT

Background: Pediatric B-cell acute lymphoblastic leukemia (B-ALL) remains a major childhood malignancy in which interactions between leukemic cells and the immune microenvironment influence disease progression and clinical outcomes. However, the temporal dynamics of soluble immune mediators during remission chemotherapy and their prognostic value remain incompletely understood. **Methods:** Here, we profiled 48 soluble immune mediators in peripheral blood (PB) and bone marrow (BM) from 36 pediatric B-ALL patients at diagnosis (D0) and during remission chemotherapy (D15, D35, and D84) using multiplex assays. Mediator profiles were also compared between patients who achieved remission (RG) and those who died during induction therapy (DG). **Results:** At D0, pediatric B-ALL patients exhibited a broadly dysregulated immune landscape, followed by progressive

remodeling throughout remission chemotherapy, with only partial normalization of mediator levels and persistent disruption of immune interaction networks over time. Patients in the DG displayed a more exacerbated immune profile at diagnosis than those in the RG. Decision tree models identified small panels of soluble immune mediators at D0 (PB: CCL5, IL-6, CXCL9, and IL-2Rα; BM: CXCL12 and CCL4) that discriminated clinical outcome with high internally resampled performance (PB: AUC = 0.996, 95% CI 0.987–1.000; BM: AUC = 0.910, 95% CI 0.790–1.000). **Conclusions:** Together, these findings provide a comprehensive characterization of longitudinal immune remodeling in pediatric B-ALL and identify candidate immune mediator panels associated with adverse clinical outcomes. These results support the further evaluation of immune profiling as a candidate approach for early risk stratification in pediatric B-ALL.

Keywords: B-cell acute lymphoblastic leukemia; tumor microenvironment; immune signatures; immune biomarkers; risk stratification.

INTRODUCTION

Acute Lymphoblastic Leukemia (ALL) is the most common childhood malignancy, accounting for approximately 30% of all pediatric cancer diagnoses, with B-cell ALL (B-ALL) comprising 85% of ALL cases (1). Despite significant therapeutic advances raising overall survival rates to over 90% in high-income countries, outcomes remain substantially worse in low- and middle-income regions (2). Furthermore, a considerable proportion of patients still experience unfavorable outcomes, including treatment resistance, relapse, and treatment-related mortality, with cure often associated with significant short- and long-term toxicities (3). Given this scenario, the identification of biomarkers to enable more precise

risk stratification at diagnosis, as well as the development of more personalized and less toxic treatment strategies, remains a critical priority in pediatric ALL.

Growing evidence demonstrates that the bone marrow (BM) microenvironment plays a crucial role in leukemic cell survival, chemoresistance, and immune evasion (4–7). A wide range of soluble immune mediators, including cytokines, chemokines, and growth factors, mediate the complex interactions between leukemic cells and components of the medullary niche (4–7). These mediators not only modulate disease progression but also influence patients' responses to therapy. Although some studies have described immune alterations in pediatric B-ALL (8–12), few have longitudinally evaluated the dynamic remodeling of these mediators in peripheral blood (PB) and BM throughout remission chemotherapy. Furthermore, the extent of immune remodeling during treatment and its potential association with clinical outcomes remain poorly understood.

To address this gap, we performed a comprehensive longitudinal analysis of 48 soluble immune mediators in paired peripheral blood and bone marrow samples from pediatric B-ALL patients. We characterized the dynamic remodeling of the immune landscape from diagnosis to the end of remission chemotherapy and investigated its relationship with clinical outcomes, including mortality during induction therapy. By integrating longitudinal and compartment-specific immune profiling, we identified candidate immune signatures and small panels of soluble immune mediators associated with adverse clinical outcomes. These findings provide a comprehensive characterization of immune remodeling in pediatric B-ALL and support the further investigation of soluble immune mediators as candidate biomarkers for early risk stratification and disease monitoring.

SUBJECTS AND METHODS

Ethics statement

This study was approved by the Research Ethics Committees of Fundação Hospitalar de Hematologia e Hemoterapia do Amazonas (HEMOAM) and Instituto René Rachou, Fundação Oswaldo Cruz (Fiocruz Minas), under approval numbers 4,982,395 and 5,022,234, respectively. Written informed consent was obtained from the parents or legal guardians of all participants prior to enrollment, and assent was obtained from the children whenever applicable. The study was conducted in accordance with the principles of the Declaration of Helsinki and the Brazilian National Health Council Resolution No. 466/2012.

Patients and control subjects

The study population comprised 36 consecutive children (<15 years) newly diagnosed with B-ALL at Fundação HEMOAM, the regional referral center for hematological diseases in the Brazilian Amazon. Diagnosis was established according to the World Health Organization classification criteria (13). Patients were prospectively followed from diagnosis through the completion of remission chemotherapy, with peripheral blood (PB) and bone marrow (BM) samples collected at predefined treatment time points.

Patients were stratified into two outcome-based groups: remission group (RG), including those who completed remission chemotherapy, and deceased group (DG), including those who died during induction therapy. The RG included 25 patients (13 males and 12 females; median age, 5 years [IQR, 3–9]), whereas the DG included 11 patients (4 males and 7 females; median age, 3 years [IQR, 1–7]).

In addition, 25 children without leukemia were included as a control group (CG) (14 males and 11 females; median age, 9 years [IQR, 5–11]). PB samples were collected from controls to provide reference values, as BM aspiration is an invasive procedure. Control

112 subjects had no history of infection within four weeks prior to sampling and showed no
113 hematological abnormalities.

114 Demographic, clinical, and laboratory characteristics of the study population are
115 summarized in **Table 1**, whereas detailed hematological parameters at diagnosis are
116 presented in **Supplementary Table 1**.

117 **Table 1. Demographic, clinical and laboratory characteristics of the study population.**

Variables	CG (n=25)		B-ALL (n=36)		Outcome during treatment				p-value
					RG (n=25)		DG (n=11)		
Age in years	9 (5 - 11)		5 (3 - 7)		5 (3 - 9)		3 (1 - 7)		0.275
Sex									
Male	14	(56%)	17	(47%)	13	(52%)	4	(36%)	0.032
Female	11	(44%)	19	(53%)	12	(48%)	7	(64%)	
Immunophenotyping									
Common B-ALL ($CD10^+$)	-	-	36	(100%)	25	(100%)	11	(100%)	NA
Aberrant markers									
Absent	-	-	26	(72%)	17	(68%)	9	(82%)	0.033
Present	-	-	10	(28%)	8	(32%)	2	(18%)	
High-risk cytogenetic findings									
Absent	-	-	24	(67%)	17	(68%)	7	(64%)	
Present	-	-	3	(8%)	3	(12%)	0	(0%)	<0.001
Missing data	-	-	9	(25%)	5	(20%)	4	(36%)	
CNS infiltration									
Absent	-	-	31	(86%)	23	(92%)	11	(100%)	
Present	-	-	2	(6%)	2	(8%)	0	(0%)	0.007
Missing data	-	-	3	(8%)	0	(0%)	0	(0%)	
Risk stratification at D0									
Low risk	-	-	9	(25%)	6	(24%)	3	(27%)	
Intermediate risk	-	-	15	(42%)	13	(52%)	2	(18%)	<0.001
High risk	-	-	12	(33%)	6	(24%)	6	(55%)	
Measurable residual disease at D15									
Negative	-	-	21	(58%)	21	(84%)	0	(0%)	
Positive	-	-	4	(11%)	4	(16%)	0	(0%)	NA
Not performed	-	-	11	(31%)	0	(0%)	11	(100%)	
Myelogram									
D0									
M1	-	-	0	(0%)	0	(0%)	0	(0%)	
M2	-	-	0	(0%)	0	(0%)	0	(0%)	>0.999
M3	-	-	36	(100%)	25	(100%)	11	(100%)	
D35									

M1	-	-	15	(42%)	15	(60%)	0	(0%)	
M2	-	-	0	(0%)	0	(0%)	0	(0%)	NA
M3	-	-	0	(0%)	0	(0%)	0	(0%)	
Not performed	-	-	21	(58%)	10	(40%)	11	(100%)	
D84									
M1	-	-	21	(58%)	21	(84%)	0	(0%)	
M2	-	-	0	(0%)	0	(0%)	0	(0%)	NA
M3	-	-	0	(0%)	0	(0%)	0	(0%)	
Not performed	-	-	15	(42%)	4	(16%)	11	(100%)	
Lymphoblast Count									
D0	-	-	32.664	(64%)	34.292	(70%)	16.800	(58%)	0.636
D35	-	-	100	(1.2%)	100	(1.2%)	-	-	NA
D84	-	-	108	(0.4%)	108	(0.4%)	-	-	NA

Abbreviations: B-ALL, B-cell acute lymphoblastic leukemia; RG, remission group (patients who completed remission chemotherapy); DG, deceased group (patients who died during induction therapy); CNS, central nervous system; M1, <5% lymphoblasts; M2, 5–25% lymphoblasts; M3, >25% lymphoblasts; NA, not applicable.

Study groups: The overall B-ALL cohort (n=36) comprises all patients included in the study and was used for analyses comparing patients with controls, whereas outcome-based analyses were performed between RG and DG.

Data presentation: Data are presented as number (percentage), unless otherwise specified.

High-risk cytogenetic findings observed in the study cohort included translocation t(9;22)(q34;q11) (Philadelphia chromosome, BCR::ABL1) and inversion inv(16)(p13;q22) with myeloid co-expression (14).

Lymphoblast count: At diagnosis (D0), results are expressed as absolute lymphoblast counts, calculated as follows: lymphoblast percentage obtained by flow cytometry multiplied by the total leukocyte count obtained by a hematological analyzer, divided by 100. At D35 and D84, lymphoblast counts are expressed as the number of lymphoblasts per 500 nucleated bone marrow cells evaluated by cytomorphological analysis. These measurements reflect different methodological approaches and are therefore not directly comparable.

Treatment regimen

All pediatric patients with B-ALL received remission chemotherapy according to the Brazilian Group for Treatment of Childhood Leukemia protocol (GBTLI-2009) (15). Remission induction therapy was designed to achieve complete remission, defined as <5% lymphoblasts in the BM after five weeks of treatment. Patients in the RG subsequently proceeded to consolidation therapy according to the same protocol.

The treatment regimen included prednisone, dexamethasone, vincristine, daunorubicin, L-asparaginase, and intrathecal therapy (MADIT: methotrexate, cytarabine, and dexamethasone), administered according to protocol specifications.

Biological sample collection

PB and BM samples were collected from B-ALL patients by venipuncture and iliac crest aspiration, respectively, at four time points: diagnosis (D0), day 15 of induction therapy (D15), end of induction therapy (D35), and day 84 of consolidation therapy (D84). In controls, PB samples were collected at a single time point.

Samples were collected into EDTA tubes (BD Vacutainer® K2EDTA) and centrifuged at 600 × g for 10 minutes at room temperature. Plasma was separated and stored at −80 °C until analysis. Samples were subsequently shipped to Fiocruz-Minas for immune mediator measurements.

A detailed methodological workflow, including patient inclusion, sampling time points, and processing procedures, is provided in **Supplementary Figure 1**.

Sample preparation and immune mediator measurement via multiplex assay

Soluble immune mediators were quantified using a multiplex bead-based assay (Bio-Plex Pro Human Cytokine Screening Panel, 48-Plex; Bio-Rad, cat. no. 12007283). The panel included chemokines, pro-inflammatory cytokines, regulatory cytokines, and growth factors (**Supplementary Table 2**).

Plasma samples were thawed at 37 °C, vortexed, and centrifuged at 14,000 × g for 5 minutes at room temperature. Assays were performed according to the manufacturer's instructions. Briefly, 50 µL of diluted bead mixture was added to each well, followed by 50 µL of sample. Plates were washed and incubated overnight at 4 °C with agitation. Detection antibody and streptavidin-phycoerythrin were subsequently added, with incubation steps performed at room temperature under agitation and protected from light. After final washes, beads were resuspended in assay buffer prior to acquisition.

Data were acquired using a Bio-Plex 200 system with xPONENT software (version 3.1). Median fluorescence intensity (MFI) values were converted to concentrations (pg/mL) using standard curves fitted with a five-parameter logistic model in Bio-Plex Manager software (version 6.2; Bio-Rad).

Conventional statistical analysis

Comparisons between B-ALL patients and controls, as well as between RG and DG, were performed using Student's t-test or the Mann–Whitney U test, as appropriate. Comparisons across time points (D0, D15, D35, and D84) were performed using one-way repeated-measures ANOVA with Tukey's post hoc test or the Friedman test with Dunn's post hoc test, as appropriate.

Data normality was assessed using the Shapiro–Wilk test. All tests were two-sided, and a p-value < 0.05 was considered statistically significant. Statistical analyses were

performed using GraphPad Prism (version 10.1.2; GraphPad Software, San Diego, CA, USA).

Heatmap analysis

Heatmaps were generated to visualize the distribution of soluble immune mediator levels across study groups and time points. Data from 48 mediators were organized by functional class (chemokines, pro-inflammatory cytokines, regulatory cytokines, and growth factors), and samples were arranged by group or time point, with clustering applied within each subset.

Values were standardized per mediator using row-wise Z-score transformation within each compartment (PB or BM) and time point, when applicable, to enable comparison across samples. To reduce the influence of extreme values, Z-scores were winsorized to a range of −3 to +3. Missing values were imputed using the median for each mediator.

Unsupervised hierarchical clustering was applied to order samples based on similarity patterns. Heatmaps were generated in R (version 4.5.1) using the *ComplexHeatmap* package, with the circlize package used for color scaling. Visualizations highlight relative differences in mediator abundance, with red and blue indicating relatively higher and lower values, respectively.

Latent variable analysis

Partial Least Squares–Discriminant Analysis (PLS-DA) was performed to explore patterns of separation between RG and DG based on soluble immune mediator profiles, with separate models constructed for PB and BM using the *mixOmics* framework. Data were centered and scaled prior to analysis.

Model performance and optimal complexity were assessed using repeated 5-fold cross-validation (50 repeats), with evaluation based on the balanced error rate (BER). Key contributors to group separation were identified based on the loadings of the first latent variable (LV1).

Signatures and delta analysis

Signature analysis was performed as previously described (Magalhães-Gama et al., 2024) (16). Continuous values for each mediator were converted into categorical variables using global median cut-offs calculated separately for each analytical comparison (B-ALL vs controls and B-ALL RG vs B-ALL DG). Individuals were classified as having lower (below the cut-off) or higher (above the cut-off) levels of each mediator. Cut-off values (pg/mL) are provided in **Supplementary Table 3**.

To assess group-level patterns, mediators were grouped by functional class (chemokines, pro-inflammatory cytokines, regulatory cytokines, and growth factors), and the proportion of individuals above the median cut-off was calculated for each group. Differences between groups were evaluated using Fisher's exact test.

Delta signatures were computed as the difference in proportions of individuals above the cut-off between groups and were also assessed using Fisher's exact test ($p < 0.05$). Results were visualized using line plots and lollipop charts according to mediator class. Venn diagrams were generated to identify shared and group-specific mediators.

Biological networks

Biological network analysis was performed to evaluate correlations among chemokines, pro-inflammatory cytokines, regulatory cytokines, and growth factors in B-ALL

patients and controls, as well as between RG and DG. Correlations between mediator levels were assessed using Spearman's rank correlation coefficient in GraphPad Prism (version 10.1.2; GraphPad Software, San Diego, CA, USA), with statistical significance set at $p < 0.05$. Significant strong correlations ($r > 0.68$) were used to construct networks in Cytoscape (version 3.10.3; National Institute of General Medical Sciences, Bethesda, MD, USA).

Correlations were represented as edges connecting nodes (mediators), with node size proportional to the number of connections. The networks were organized using circular layouts and grouped according to functional classes. Connectivity was further quantified by calculating the total number and relative proportion of significant correlations within each mediator class and compared across groups.

Decision Tree Analysis

To investigate the association between soluble immune mediators and clinical outcomes in pediatric B-ALL, an interpretable decision tree model was developed based on baseline (D0) measurements from PB and BM. Feature selection was performed using a Random Forest algorithm with 500 trees and 20-fold cross-validation, incorporating the Synthetic Minority Oversampling Technique (SMOTE) to address class imbalance between RG and DG. Variable importance was estimated using the mean decrease in Gini index.

To assess robustness, bootstrap resampling (50 iterations) was applied, and the average variable importance across iterations was used to select the top 10 predictors. These variables were then used to construct a decision tree using the *rpart* package in R.

Model performance was evaluated using receiver operating characteristic (ROC) curves and confusion matrices, with performance metrics including sensitivity, specificity, balanced accuracy, and F1-score. The classification threshold was optimized to balance

sensitivity and specificity. Performance metrics were reported with 95% confidence intervals (95% CI), when applicable. The same analytical workflow was applied to BM data.

RESULTS

Systemic immune landscape at diagnosis in pediatric B-ALL

At D0, pediatric B-ALL patients exhibited a markedly altered systemic immune mediator profile compared to controls (**Figure 1**). A broad increase in soluble mediators was observed, consistent with a mixed inflammatory signature.

Elevated levels were detected across multiple mediator classes, including chemokines (e.g., CCL2, CCL3, CXCL8, CXCL9, CXCL10), pro-inflammatory cytokines (e.g., IL-1β, IL-6, TNF-α, IFN-γ, IL-17, IL-18), regulatory cytokines (e.g., IL-4, IL-5, IL-9, IL-10), and growth factors (e.g., bFGF, HGF, SCGF-β, G-CSF, GM-CSF, IL-2Rα, MIF). Notably, VEGF was the only mediator reduced in B-ALL patients relative to controls, contrasting with the overall pattern of increased mediator levels.

Together, these findings indicate a broadly activated and dysregulated immune landscape at D0, involving the simultaneous engagement of inflammatory, regulatory, and growth-related axes, with a distinct divergence in the VEGF-associated pathway.

Structured and heterogeneous immune mediator landscape distinguishes pediatric B-ALL from controls at diagnosis

At D0, heatmap analysis revealed a clear separation between controls and pediatric B-ALL patients, with the latter displaying a broadly elevated profile of soluble immune mediators across all functional classes (**Figure 2**).

Importantly, the B-ALL group exhibited marked inter-individual heterogeneity, with variable patterns of mediator expression across patients rather than a uniform increase, consistently observed across chemokines, pro-inflammatory cytokines, regulatory cytokines, and growth factors. The coordinated elevation of multiple mediator classes further suggests a structured, multi-axis immune response rather than isolated changes in individual analytes.

These patterns were further supported by signature analysis, which revealed a higher proportion of individuals with increased mediator levels across all functional classes in B-ALL patients compared to controls (**Supplementary Figure 2**).

Together, these findings indicate that the systemic immune response in pediatric B-ALL at D0 is not only amplified but also highly organized and heterogeneous, supporting the presence of distinct immune mediator patterns across patients.

Distinct temporal remodeling of immune mediator profiles in peripheral blood and bone marrow during treatment in pediatric B-ALL

Heatmap analysis revealed dynamic changes in soluble immune mediator profiles throughout treatment in pediatric B-ALL (**Figure 3**). At D15, both PB (**Figure 3A**) and BM (**Figure 3B**) exhibited a marked attenuation of the elevated mediator profile observed at D0.

At D35, this pattern shifted, with a partial re-emergence of elevated mediator levels, particularly evident in BM, where broader and more pronounced regions of increased expression were observed. In contrast, PB showed a more limited and heterogeneous reconfiguration.

By D84, PB profiles converged toward a more homogeneous pattern characterized by predominantly neutral to reduced expression levels. Conversely, BM retained localized clusters of elevated mediator expression, maintaining a higher degree of heterogeneity.

These kinetic patterns were further supported by longitudinal analysis of individual mediator levels in PB, confirming a non-linear pattern of early reduction, intermediate reconfiguration, and late attenuation (**Supplementary Figure 3**). In contrast, BM analysis revealed more heterogeneous and non-uniform temporal patterns, reinforcing compartment-specific immune remodeling (**Supplementary Figure 4**).

Together, these findings indicate distinct compartment-specific remodeling dynamics, with PB undergoing rapid and more uniform normalization, whereas BM exhibits sustained and heterogeneous immune activity during treatment, suggesting incomplete restoration of immune homeostasis.

Marked reduction in immunological interactions and central role of IL-10 in biological networks in pediatric B-ALL

Biological network analysis revealed a marked reduction in the number of significant correlations in both PB and BM of B-ALL patients compared to controls (**Figure 4**). This reduction persisted throughout treatment and was not restored by D84, indicating sustained disruption of immune mediator interactions.

In PB, the remaining network structure showed a predominance of correlations associated with growth factors, including a predominance of negative correlations involving VEGF. In contrast, BM networks were characterized by an even lower connectivity and a predominance of interactions involving pro-inflammatory and regulatory cytokines, highlighting distinct compartment-specific interaction patterns.

Notably, the regulatory cytokine IL-10 emerged as the most connected mediator in both compartments, establishing the highest number of correlations and suggesting a central

role in network organization. In contrast, VEGF displayed an opposing interaction profile, being predominantly associated with negative correlations within the network.

When comparing patients who achieved remission (RG) and those who died during induction therapy (DG), no major differences in overall network connectivity were observed (**Supplementary Figure 5**), and heatmap analysis similarly showed no clear group-specific separation (**Supplementary Figure 6**). Correlation analysis between immune mediators and leukemic blast counts at D0 identified only one strong and significant association, involving PDGF (**Supplementary Figure 7**).

Together, these findings indicate a sustained disruption and reorganization of immune mediator interactions in pediatric B-ALL, with distinct compartment-specific patterns, a central role for IL-10 in network connectivity, and a divergent interaction profile associated with VEGF.

Baseline immune mediator profiles differ according to clinical outcome in pediatric B-ALL

To identify mediators associated with adverse clinical outcomes, we compared soluble immune mediator profiles at D0 between RG and DG (**Figure 5**).

Overall, DG displayed higher levels of multiple soluble immune mediators than those in the RG, with increases spanning several functional classes, including chemokines, pro-inflammatory cytokines, regulatory cytokines, and growth factors. Representative increases included CCL4, CCL5, CCL11, CXCL8, IFN-γ, IL-4, IL-9, HGF, PDGF, and IL-2Rα.

Conversely, several mediators were reduced in DG, most notably VEGF in both PB and BM, along with IL-7 in PB and selected chemokines and cytokines in BM. Notably,

VEGF showed a consistent reduction across compartments, contrasting with the broadly elevated mediator profile observed in DG.

While these differences highlight distinct immune mediator profiles between outcome groups, latent variable analysis further revealed a clearer discrimination between RG and DG, particularly in BM, suggesting that combinatorial mediator patterns may better capture the immune heterogeneity associated with clinical outcome than individual mediators (**Supplementary Figure 8**).

Immunological signatures reveal dysregulated mediator patterns associated with clinical outcome in pediatric B-ALL

To further characterize the immune profile of DG patients and identify candidate immune signatures associated with clinical outcome, immunological signatures were constructed at D0 and integrated with delta analysis (**Figure 6**).

In PB, DG exhibited a higher proportion of individuals with elevated mediator levels across all functional classes. In BM, a more heterogeneous pattern was observed, with increased chemokine production accompanied by reduced representation of regulatory cytokines (**Figure 6A**).

Delta analysis further identified a broad set of mediators differentially regulated in DG compared to RG, spanning multiple functional classes (**Figure 6B**). Representative mediators included chemokines (e.g., CCL3, CCL4, CCL5, CXCL9), pro-inflammatory cytokines (e.g., IL-6, TNF-α, TNF-β, IFN-γ), regulatory cytokines (e.g., IL-9, IL-10), and growth factors (e.g., HGF, PDGF, G-CSF, IL-2Rα), with both increased and decreased patterns observed across compartments.

The Venn diagram highlighted both shared and compartment-specific mediators, identifying a subset of overlapping candidates between PB and BM that may represent promising candidate biomarkers requiring further validation (**Figure 6C**). Notably, these shared mediators reflect consistent alterations across compartments, supporting their further evaluation as candidate biomarkers associated with adverse clinical outcomes. Additionally, class-based signature analysis reinforced these findings, demonstrating a globally exacerbated and imbalanced immune mediator profile in DG patients (**Figure 6D**).

Together, these findings identify candidate immune signatures associated with adverse clinical outcomes and provide a rationale for further investigation of soluble immune mediators as biomarkers for risk stratification in pediatric B-ALL.

Decision tree models identify candidate immune mediator panels associated with clinical outcome in pediatric B-ALL at diagnosis

To identify candidate combinations of soluble immune mediators associated with clinical outcome, decision tree models were constructed using candidate predictors identified from prior analyses at D0. Analysis of PB and BM samples identified distinct panels of soluble immune mediators that discriminated between RG and DG (**Figure 7**).

Following 50 bootstrap iterations using a Random Forest-based variable selection approach, the ten most important variables in PB were selected to construct the decision tree. Among these, CCL5, IL-6, CXCL9, and IL-2Rα emerged as key contributors, resulting in a model with 95.8% sensitivity, 100.0% specificity, a balanced accuracy of 97.9%, and an area under the curve (AUC) of 0.996 (95% CI: 0.987–1.000) (**Figure 7A**).

A similar approach applied to BM samples identified CXCL12 and CCL4 as the key variables. This model achieved 100% sensitivity, 77.8% specificity, a balanced accuracy of 88.9%, and an AUC of 0.910 (95% CI: 0.790–1.000) (**Figure 7B**).

Together, these findings identify candidate immune mediator panels with excellent discriminative performance within this cohort, supporting their further evaluation as candidate biomarkers for early risk stratification in pediatric B-ALL.

DISCUSSION

Understanding the immunological landscape of pediatric B-ALL and its relationship with clinical outcomes remains a critical challenge, as it may provide key insights into disease progression, therapeutic response, and risk stratification. In this context, our data at D0 corroborate previous findings showing that pediatric B-ALL patients exhibit an immunological imbalance at both systemic and local levels (11,12). Our findings revealed a coordinated elevation of chemokines, pro-inflammatory cytokines, regulatory cytokines, and growth factors, reflecting a broadly dysregulated immune profile. This mixed pattern likely represents a host response to leukemic expansion, coupled with immune-evasion and microenvironmental mechanisms inherent to the malignancy (17,18).

Notably, VEGF emerged as the only mediator reduced at D0 relative to controls, contrasting with reports of elevated VEGF levels in leukemia, often linked to angiogenic activation within the BM niche (19,20). This discrepancy may reflect context-dependent regulation of the VEGF axis in pediatric B-ALL, potentially involving local consumption or sequestration within the BM niche, thereby reducing its detectable levels in PB. Regional and population-specific immunogenetic backgrounds may contribute to context-dependent

differences in soluble immune mediator landscapes across pediatric B-ALL cohorts (21). In this context, the reduced systemic levels of VEGF may not reflect diminished biological activity, but rather a redistribution within the leukemic microenvironment. This interpretation is consistent with our network analysis, in which VEGF exhibited a distinct interaction profile, suggesting an altered role within the immunological architecture and reinforcing the presence of compartmentalized regulatory dynamics.

Throughout remission chemotherapy, a dynamic remodeling of the immune landscape was observed, with distinct compartment-specific patterns. PB profiles tended to converge toward a more homogeneous and attenuated state at later time points, whereas BM retained greater heterogeneity, indicating sustained immune activity within the leukemic niche. This divergence suggests that systemic immune normalization does not necessarily reflect processes occurring within the primary disease site. Importantly, this apparent normalization in PB did not correspond to restoration of coordinated immune regulation, as biological networks remained markedly reduced throughout treatment. Together, these findings indicate that immune remodeling during therapy is partial and compartmentalized, with incomplete restoration of immune homeostasis.

These observations are consistent with studies demonstrating persistent inflammatory activity following induction therapy, including sustained elevations of TNF-α and IFN-γ even in hematological remission (22). Long-term follow-up further shows that clinically cured pediatric ALL survivors exhibit persistent alterations in circulating immune mediators, consistent with chronic low-grade inflammation and features of premature immunological aging (23). In addition, depletion of T and B lymphocytes contributes to prolonged immunosuppression, impaired immune competence, and reduced vaccine responsiveness (24). Together, these findings indicate that immune dysregulation persists

beyond treatment, reinforcing that clinical remission does not equate to full immunological recovery and supporting continued immunological monitoring and tailored vaccination strategies in pediatric ALL survivors.

This persistent immune dysregulation aligns with previous studies showing extensive remodeling of the B-ALL microenvironment, in which leukemic blasts manipulate immune checkpoints and soluble signaling pathways to promote survival and immune evasion (17,25,26). In line with this, our findings show that BM mediator dynamics are more heterogeneous than in PB, indicating that peripheral profiles only partially reflect processes within the bone marrow niche. In parallel, network analysis revealed a sustained reduction in immune interactions in B-ALL patients. Within this context, IL-10 emerged as a highly connected node, suggesting the involvement of a regulatory axis during disease progression and therapy, consistent with its established role in leukemia biology (27). As correlation-based networks do not imply causality, these findings reflect altered immune interaction structures.

Patients with fatal outcomes during induction therapy exhibited a more exacerbated and dysregulated immune profile at D0, characterized by increased levels across multiple mediator classes, including chemokines, pro-inflammatory cytokines, regulatory cytokines, and growth factors, compared with RG. This broad activation pattern suggests that adverse clinical outcomes may be associated with coordinated multi-axis immune dysregulation rather than alterations in isolated mediators, reflecting marked immune dysregulation at disease onset. Notably, these immunological differences occurred alongside distinct clinical and hematological features at D0, including a higher leukemic burden in the peripheral circulation and a greater proportion of high-risk patients, consistent with a more advanced and systemically disseminated disease phenotype associated with immune dysregulation.

In this context, an important objective of this study was to investigate whether baseline immune profiles contain candidate immune signatures associated with mortality in pediatric B-ALL. Decision tree analysis identified small panels of soluble mediators in PB (CCL5, IL-6, CXCL9, and IL-2Rα) and BM (CXCL12 and CCL4) that effectively discriminated between RG and DG at D0, with strong internally resampled performance. Notably, the PB panel required a broader combination of mediators yet achieved higher discriminative performance, whereas the BM panel relied on fewer mediators with slightly lower performance, suggesting a more distributed signal in PB and a more concentrated, niche-driven signature in BM. Complementary latent variable modeling supported the presence of outcome-associated multivariate structure, with a modest tendency toward greater separation in BM than in PB, highlighting the role of the leukemic niche in shaping clinically relevant immune patterns.

Importantly, these findings highlight the advantage of combinatorial immune mediator signatures over single mediators, reflecting the complex and multi-axis nature of immune dysregulation in B-ALL. While BM findings emphasize the biological relevance of the leukemic niche, PB-based panels suggest the feasibility of a minimally invasive approach for future immune-based risk assessment. Moreover, such signatures may provide complementary immune-related information beyond conventional clinical or molecular parameters. This is particularly relevant in pediatric B-ALL, where early identification of high-risk patients remains challenging. Together, these results support the further evaluation of immune profiling at D0 as a candidate approach for early risk stratification and provide a rationale for future validation studies exploring its potential clinical utility.

Despite the strengths of the study, several limitations should be acknowledged. The relatively small sample size, particularly in the DG, may limit statistical power and

generalizability, warranting validation in larger, multicenter cohorts. The lack of healthy BM controls precluded the definition of a true physiological baseline, although this may be addressed using public datasets or alternative comparator groups. In addition, our analyses were restricted to soluble mediators without cellular phenotyping, limiting mechanistic insight. Furthermore, the lack of comprehensive cytogenetic and molecular profiling limited further exploration of the relationship between immune signatures and established genetic risk features. Finally, although decision tree models offer clinical interpretability, their performance requires validation in independent cohorts, comparison with other machine learning approaches, and assessment of their added value beyond established clinical and molecular risk parameters.

In summary, our study shows that pediatric B-ALL is characterized by a dynamic, persistently dysregulated immunological landscape throughout remission chemotherapy, with distinct compartment-specific remodeling patterns in PB and BM. While PB profiles converge toward a more attenuated state, BM retains greater heterogeneity, reflecting sustained immune activity within the leukemic niche. Importantly, this apparent normalization does not correspond to restoration of coordinated immune regulation. Moreover, DG exhibited a more exacerbated immune profile at D0, reflected in distinct immune signatures and candidate immune mediator panels associated with adverse clinical outcomes. Together, these findings provide a comprehensive characterization of immune remodeling in pediatric B-ALL and support the further evaluation of immune signatures as candidate biomarkers for early risk stratification and future precision medicine approaches.

LIST OF ABBREVIATIONS

ALL, Acute Lymphoblastic Leukemia; AUC, Area Under the Curve; B-ALL, B-cell Acute Lymphoblastic Leukemia; BM, bone marrow; CG, control group; CNS, central nervous system; DG, decease group (patients who died during induction therapy); RG, remission group (patients who completed remission chemotherapy); D0, diagnosis (baseline); D15, day 15 of induction therapy; D35, end of induction therapy; D84, day 84 of consolidation therapy; IQR, interquartile range; LV, latent variable; MFI, mean fluorescence intensity; PB, peripheral blood; PLS-DA, Partial Least Squares-Discriminant Analysis; ROC, Receiver Operating Characteristic; RT, room temperature; SAPE, streptavidin-phycoerythrin; SMOTE, Synthetic Minority Oversampling Technique.

DECLARATIONS

Ethics approval and consent to participate

The study was conducted in accordance with the Declaration of Helsinki and approved by the appropriate institutional and national ethics committees. Written informed consent was obtained from the parents or legal guardians of all participants prior to enrollment.

Consent for publication

Written informed consent for the publication of anonymized data was obtained from the parents or legal guardians of all participants.

Data availability statement

The original contributions presented in this study are included in the article and its supplementary material. Further inquiries can be directed to the corresponding author(s).

Supplementary material

The Supplementary Material for this article can be found online at: https://doi.org/

Supplementary Table 1. Hematological parameters at diagnosis in pediatric B-ALL patients and controls.

Supplementary Table 2. Soluble immune mediators included in the multiplex panel and their classification.

Supplementary Table 3. Global baseline median cutoff values for soluble immune mediators (pg/mL).

Supplementary Figure 1. Study Flowchart detailing Population inclusion, Sample collection, and processing from pediatric patients with B-cell acute lymphoblastic leukemia and healthy controls.

Supplementary Figure 2. Signature of soluble immune mediators in peripheral blood of pediatric B-ALL patients at diagnosis compared to controls.

Supplementary Figure 3. Kinetics of soluble immune mediators in the peripheral blood of pediatric B-ALL patients at diagnosis and during remission chemotherapy.

Supplementary Figure 4. Kinetics of soluble immune mediators in the bone marrow of pediatric B-ALL patients at diagnosis and during remission chemotherapy.

Supplementary Figure 5. Biological network comparison between remission and deceased pediatric B-ALL patients at diagnosis.

Supplementary Figure 6. Immune mediator heatmap comparison between remission and deceased pediatric B-ALL patients at diagnosis.

Supplementary Figure 7. Correlation matrix of blasts and soluble immunological mediators in pediatric B-ALL patients at diagnosis.

Supplementary Figure 8. Latent variable analysis reveals outcome-associated immune mediator signatures in pediatric B-ALL.

Competing interests

The authors declare no competing interests.

Funding

Financial support was provided by Fundação de Amparo à Pesquisa do Estado do Amazonas (FAPEAM) (Pró-Estado Program #002/2008, #007/2018, and #005/2019; POSGRAD Program #002/2025), Conselho Nacional de Desenvolvimento Científico e Tecnológico (CNPq), and Coordenação de Aperfeiçoamento de Pessoal de Nível Superior (CAPES) (PROCAD-Amazônia 2018 Program #88881.200581/2018-01; PDPG-CONSOLIDACAO-3-4 Program #88887.707248/2022-00). FM-G received a PhD fellowship from FAPEAM (POSGFE Program #012/2021). FSS, CLSC, JSM, and JCFN received PhD fellowships from FAPEAM and CAPES. ICF and MSB received Master's fellowships from FAPEAM and CAPES. JGSG received an undergraduate research

fellowship from FAPEAM (PAIC Program). OAM-F, AGC, AM, and AT-C are research fellows of CNPq. OAM-F is also a research fellow supported by Universidade do Estado do Amazonas (PROVISIT No. 005/2023-PROPESP/UEA). The funders had no role in study design, data collection and analysis, decision to publish, or preparation of the manuscript.

Author contributions

FM-G, AT-C, AGC, and OAM-F designed and performed the experiments, analyzed the data, and wrote the manuscript. FM-G, IAC-R, GRF, GMSP, and OAM-F analyzed the data. FSS, MSB, ICF, JSM, JCFN, CLSC, JGSG, NDA, FSAH, DAO, ACC-A, MPSS, AMT, and AM recruited participants, performed the experiments, and revised the manuscript. OAM-F, AGC, and AT-C supervised the project, designed the experiments, interpreted the data, and revised the manuscript. All authors read and approved the final version of the manuscript.

Acknowledgments

The authors thank the Department of Education and Research at HEMOAM for the use of its facilities and infrastructure, as well as the Program for Technological Development in Tools for Health-RPT-FIOCRUZ for access to the Flow Cytometry facility at FIOCRUZ-Minas and the financial support provided by FAPEMIG (APQ-03113-24).

We also thank the Grupo Amazônico de Pesquisa Interdisciplinar em Saúde (Amazon InterScience) at Universidade Federal do Amazonas (UFAM), particularly the project team “Cellular and Molecular Biomarkers Involved in the Immunological Response of Patients with Acute Lymphoblastic Leukemia: New Approaches Applied to Diagnosis, Prognosis, and Therapeutics (CMB-ALL)”, in partnership with the HEMOAM collection team, for their

invaluable collaboration in sample acquisition, processing, and storage, as well as for improving routine procedures for patients under treatment.

Additionally, we acknowledge the Grupo Integrado de Pesquisas em Biomarcadores (GIPB) at Instituto René Rachou, Fundação Oswaldo Cruz (FIOCRUZ-Minas), for their excellent technical assistance and support with assays and analyses.

Finally, we are deeply grateful to all participating patients and controls, as well as their parents and legal guardians, whose willingness to participate made this study possible.

REFERENCES

1. Hunger SP, Lu X, Devidas M, Camitta BM, Gaynon PS, Winick NJ, et al. Improved Survival for Children and Adolescents With Acute Lymphoblastic Leukemia Between 1990 and 2005: A Report From the Children's Oncology Group. J Clin Oncol [Internet]. 2012 May 10;30(14):1663–9. Available from: https://ascopubs.org/doi/10.1200/JCO.2011.37.8018

2. Magrath I, Steliarova-Foucher E, Epelman S, Ribeiro RC, Harif M, Li C-K, et al. Paediatric cancer in low-income and middle-income countries. Lancet Oncol [Internet]. 2013 Mar;14(3):e104–16. Available from: https://linkinghub.elsevier.com/retrieve/pii/S1470204513700081

3. Jasinski S, De Los Reyes FA, Yametti GC, Pierro J, Raetz E, Carroll WL. Immunotherapy in Pediatric B-Cell Acute Lymphoblastic Leukemia: Advances and Ongoing Challenges. Pediatr Drugs [Internet]. 2020 Oct 29;22(5):485–99. Available from: https://link.springer.com/10.1007/s40272-020-00413-3

4. Chiarini F, Lonetti A, Evangelisti C, Buontempo F, Orsini E, Evangelisti C, et al. Advances in understanding the acute lymphoblastic leukemia bone marrow microenvironment: From biology to therapeutic targeting. Biochim Biophys Acta - Mol Cell Res [Internet]. 2016;1863(3):449–63. Available from: http://dx.doi.org/10.1016/j.bbamcr.2015.08.015

5. Tabe Y, Konopleva M. Advances in understanding the leukaemia microenvironment. Br J Haematol [Internet]. 2014 Mar;164(6):767–78. Available from: http://doi.wiley.com/10.1111/bjh.12725

6. Hughes AM, Kuek V, Kotecha RS, Cheung LC. The Bone Marrow Microenvironment in B-Cell Development and Malignancy. Cancers (Basel) [Internet]. 2022 Apr 22;14(9):2089. Available from: https://www.mdpi.com/2072-6694/14/9/2089

7. Meyer LK, Hermiston ML. The bone marrow microenvironment as a mediator of chemoresistance in acute lymphoblastic leukemia. Cancer Drug Resist [Internet]. 2019; Available from: https://www.oaepublish.com/articles/cdr.2019.63

8. Luczyński W, Stasiak-Barmuta A, Krawczuk-Rybak M, Malinowska I. Assessment of selected co-stimulatory, adhesion and activatory molecules and cytokines of Th(1)/Th(2) balance in acute lymphoblastic leukemia in children. Arch Immunol Ther Exp (Warsz) [Internet]. 2005;53(4):357–63. Available from: http://www.ncbi.nlm.nih.gov/pubmed/16088321

9. Horacek JM, Kupsa T, Vasatova M, Jebavy L, Zak P. Evaluation of serum levels of multiple cytokines and adhesion molecules in patients with newly diagnosed acute lymphoblastic leukemia using biochip array technology. Exp Oncol. 2013;35(3):229–

30.

10. Dai Q, Zhang G, Wang Y, Ye L, Shi R, Peng L, et al. Cytokine network imbalance in children with B-cell acute lymphoblastic leukemia at diagnosis. Cytokine. 2023 Sep;169:156267.

11. Magalhães-Gama F, Kerr MWA, de Araújo ND, Ibiapina HNS, Neves JCF, Hanna FSA, et al. Imbalance of Chemokines and Cytokines in the Bone Marrow Microenvironment of Children with B-Cell Acute Lymphoblastic Leukemia. Saleh R, editor. J Oncol [Internet]. 2021 Jul 22;2021:1–9. Available from: https://www.hindawi.com/journals/jo/2021/5530650/

12. Carvalho MPSS, Magalhães-Gama F, Loiola BP, Neves JCF, Araújo ND, Silva FS, et al. Systemic immunological profile of children with B-cell acute lymphoblastic leukemia: performance of cell populations and soluble mediators as serum biomarkers. Front Oncol [Internet]. 2023 Dec 1;13. Available from: https://www.frontiersin.org/articles/10.3389/fonc.2023.1290505/full

13. World Health Organization (WHO). World Health Organization Classification of Tumours of Haematopoietic and Lymphoid Tissues. Geneva, Switzerland; 2016.

14. Malard F, Mohty M. Acute lymphoblastic leukaemia. Lancet [Internet]. 2020 Apr;395(10230):1146–62. Available from: https://linkinghub.elsevier.com/retrieve/pii/S0140673619330181

15. Sociedade Brasileira de Oncologia Pediátrica. Protocolo brasileiro de tratamento da leucemia linfóide aguda na infância GBTLI LLA-2009. São Paulo, Brazil; 2011.

16. Magalhães-Gama F, Malheiros Araújo Silvestrini M, Neves JCF, Araújo ND, Alves-

Hanna FS, Kerr MWA, et al. Exploring cell-derived extracellular vesicles in peripheral blood and bone marrow of B-cell acute lymphoblastic leukemia pediatric patients: proof-of-concept study. Front Immunol [Internet]. 2024 Aug 21;15. Available from: https://www.frontiersin.org/articles/10.3389/fimmu.2024.1421036/full

17. Jiménez-Morales S, Aranda-Uribe IS, Pérez-Amado CJ, Ramírez-Bello J, Hidalgo-Miranda A. Mechanisms of Immunosuppressive Tumor Evasion: Focus on Acute Lymphoblastic Leukemia. Front Immunol [Internet]. 2021 Nov 18;12. Available from: https://www.frontiersin.org/articles/10.3389/fimmu.2021.737340/full

18. Pastorczak A, Domka K, Fidyt K, Poprzeczko M, Firczuk M. Mechanisms of Immune Evasion in Acute Lymphoblastic Leukemia. Cancers (Basel) [Internet]. 2021 Mar 26;13(7):1536. Available from: https://www.mdpi.com/2072-6694/13/7/1536

19. Aghaei M, JalaliFar MA, Yousefi-Avarvand A, Bahreiny SS, Karamali N, Mansouri Z, et al. Update Prognostic Potency of Vascular Endothelial Growth Factor-A in the Acute Lymphoblastic Leukemia Landscape: A Meta-Analysis. Cancer Rep [Internet]. 2025 Sep 13;8(9). Available from: https://onlinelibrary.wiley.com/doi/10.1002/cnr2.70351

20. Meena R, Nangia A, Sharma S, Chandra J. Serum Levels of Vascular Endothelial Growth Factor and Its Receptor in Newly Diagnosed Paediatric Acute Lymphoblastic Leukemia. Indian J Hematol Blood Transfus [Internet]. 2021 Oct 23;37(4):586–92. Available from: https://link.springer.com/10.1007/s12288-021-01413-0

21. Xabregas LA, Hanna FSA, Magalhães-Gama F, Souza GL, Pereira DS, de Lima AB, et al. Association of Toll-like receptors polymorphisms with the risk of acute

lymphoblastic leukemia in the Brazilian Amazon. Sci Rep [Internet]. 2022 Sep 7;12(1):15159. Available from: https://www.nature.com/articles/s41598-022-19130-7

22. Broto GE, Silva PRB, Trigo FC, Victorino VJ, Bonifácio KL, Pavanelli WR, et al. Impact of the induction phase chemotherapy on cytokines and oxidative markers in peripheral and bone marrow plasma of children with acute lymphocytic leukemia. Curr Res Immunol [Internet]. 2021;2:163–8. Available from: https://linkinghub.elsevier.com/retrieve/pii/S2590255521000172

23. Latoch E, Konończuk K, Konstantynowicz-Nowicka K, Muszyńska-Rosłan K, Sztolsztener K, Chabowski A, et al. Asymptomatic Survivors of Childhood Acute Lymphoblastic Leukemia Demonstrate a Biological Profile of Inflamm-Aging Early in Life. Cancers (Basel) [Internet]. 2022 May 20;14(10):2522. Available from: https://www.mdpi.com/2072-6694/14/10/2522

24. Toret E, Yel SE, Suman M, Duzenli Kar Y, Ozdemir ZC, Dinleyici M, et al. Immunization status and re-immunization of childhood acute lymphoblastic leukemia survivors. Hum Vaccin Immunother [Internet]. 2021 Apr 3;17(4):1132–5. Available from: https://www.tandfonline.com/doi/full/10.1080/21645515.2020.1802975

25. Witkowski MT, Dolgalev I, Evensen NA, Ma C, Chambers T, Roberts KG, et al. Extensive Remodeling of the Immune Microenvironment in B Cell Acute Lymphoblastic Leukemia. Cancer Cell [Internet]. 2020 Jun;37(6):867-882.e12. Available from: https://linkinghub.elsevier.com/retrieve/pii/S1535610820302142

26. Poveda-Garavito N, Combita AL. Contribution of the TIME in BCP-ALL: the basis

for novel approaches therapeutics. Front Immunol [Internet]. 2024 Jan 17;14. Available from: https://www.frontiersin.org/articles/10.3389/fimmu.2023.1325255/full

27. Silva FS, Barros-Lima A, Souza-Barros M, Crespo-Neto JA, Santos VGR, Pereira DS, et al. A dual-role for IL-10: From leukemogenesis to the tumor progression in acute lymphoblastic leukemia. Cytokine [Internet]. 2023 Nov;171:156371. Available from: https://linkinghub.elsevier.com/retrieve/pii/S1043466623002491

FIGURE LEGENDS

Figure 1. Soluble immune mediator profiles in peripheral blood of pediatric B-ALL at diagnosis. The concentrations of chemokines, pro-inflammatory cytokines, regulatory cytokines, and growth factors were measured in B-ALL patients (⬣) at diagnosis and in the control group (CG: ○). The immune mediator patterns of B-ALL patients in relation to the CG are indicated by background color: decreased levels (□), unaltered levels (□), and increased levels (□). Soluble immune mediators were quantified using a multiplex assay, as detailed in the Methods section. Data are presented as median bars with individual points displayed in scatter dot plots, expressed in picograms per milliliter (pg/mL). Statistical significance was determined using the Mann-Whitney U test, with significant differences denoted by asterisks: $*p < 0.05$, $**p < 0.01$, and $***p < 0.001$.

Figure 2. Heatmap of soluble immune mediators in pediatric B-ALL at diagnosis. The relative abundance of 48 soluble immune mediators was assessed in B-ALL patients at diagnosis (D0) and in the control group (CG). Each column represents an individual sample and each row a mediator, grouped according to functional classes (chemokines, pro-inflammatory cytokines, regulatory cytokines, and growth factors; left annotation bar). Samples were organized using unsupervised hierarchical clustering (top dendrogram), highlighting patterns across groups. Data are presented as Z-scores calculated per mediator, where red indicates higher and blue lower concentrations relative to the overall distribution (scale −3 to +3). Heatmaps were generated using the "ComplexHeatmap" package, with color scaling implemented using the "circlize" package in R. Soluble immune mediators were quantified using a multiplex assay, as described in the Methods section.

Figure 3. Heatmap of soluble immune mediators in pediatric B-ALL patients during remission chemotherapy. The relative abundance of 48 soluble immune mediators was assessed in **(A)** peripheral blood (PB) and **(B)** bone marrow (BM) at diagnosis (D0) and at three on-treatment time points (D15, D35, and D84). Each column represents an individual sample and each row a mediator, grouped according to functional classes (chemokines, pro-inflammatory cytokines, regulatory cytokines, and growth factors; left annotation bar). Samples were organized by time point and, within each time point, ordered using unsupervised hierarchical clustering (top dendrograms). Data are presented as Z-scores calculated per mediator within each compartment, where red indicates higher and blue lower concentrations relative to the overall distribution (scale −3 to +3). Heatmaps were generated using the "ComplexHeatmap" package, with color scaling implemented using the "circlize" package in R. Soluble immune mediators were quantified using a multiplex assay, as described in the Methods section.

Figure 4. Longitudinal biological networks of soluble immune mediators in pediatric B-ALL. Biological networks were assembled to identify the complex interactions among soluble immune mediators in the peripheral blood and bone marrow of pediatric B-ALL patients. The analysis was conducted at four consecutive time points of treatment: diagnosis baseline (D0), day 15 of induction therapy (D15), end of induction therapy (D35), and day 84 of consolidation therapy (D84). Correlation analysis was employed to construct biological networks according to significant "*r*" scores ($p < 0.05$) using Spearman correlation tests. Significant and strong correlations ($r > 0.68$) were used to construct the networks. A node color key was applied to identify the different classes of mediators: chemokines (●), pro-

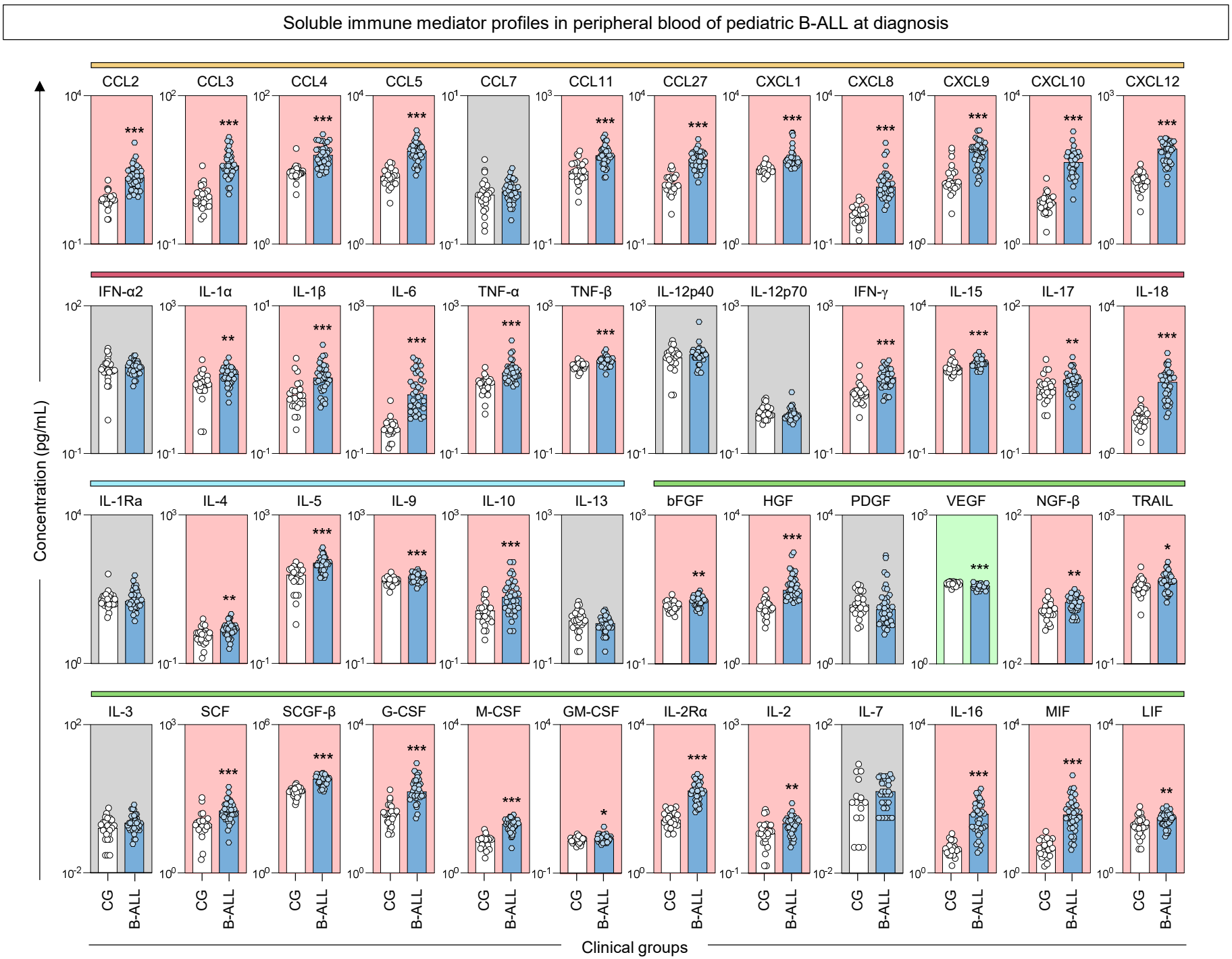
inflammatory cytokines (●), regulatory cytokines (●), and growth factors (●) in B-ALL patients and the control group (CG). Node size is proportional to the number of correlations. Connecting edges illustrate positive (gray continuous lines) and negative (red dashed lines) correlations between pairs of attributes. The circular background area is proportional to the number of correlations of each cluster within the respective network. The number of correlations observed for each network is provided in the figure and used for comparison between the time points of remission chemotherapy and the evaluated compartments.

Figure 5. Baseline immune mediator profiles according to clinical outcome in pediatric B-ALL. The concentrations of chemokines, pro-inflammatory cytokines, regulatory cytokines, and growth factors were measured in the peripheral blood (PB: ◆) and bone marrow (BM: ◆) of B-ALL patients who completed remission chemotherapy (Remission Group - RG), and in the PB (□) and BM (■) of B-ALL patients who died during induction therapy (Deceased Group - DG). The immune mediator patterns of the B-ALL DG patients in relation to the B-ALL RG are indicated by the background color: decreased levels (□); unaltered levels (□); and increased levels (□). Soluble immune mediators were quantified using a multiplex assay, as detailed in the Methods section. Data are presented as median bars with individual points displayed in scatter dot plots, expressed in picograms per milliliter (pg/mL). Statistical significance was determined using the Mann-Whitney U test, with significant differences denoted by asterisks: *$p < 0.05$, **$p < 0.01$, and ***$p < 0.001$.

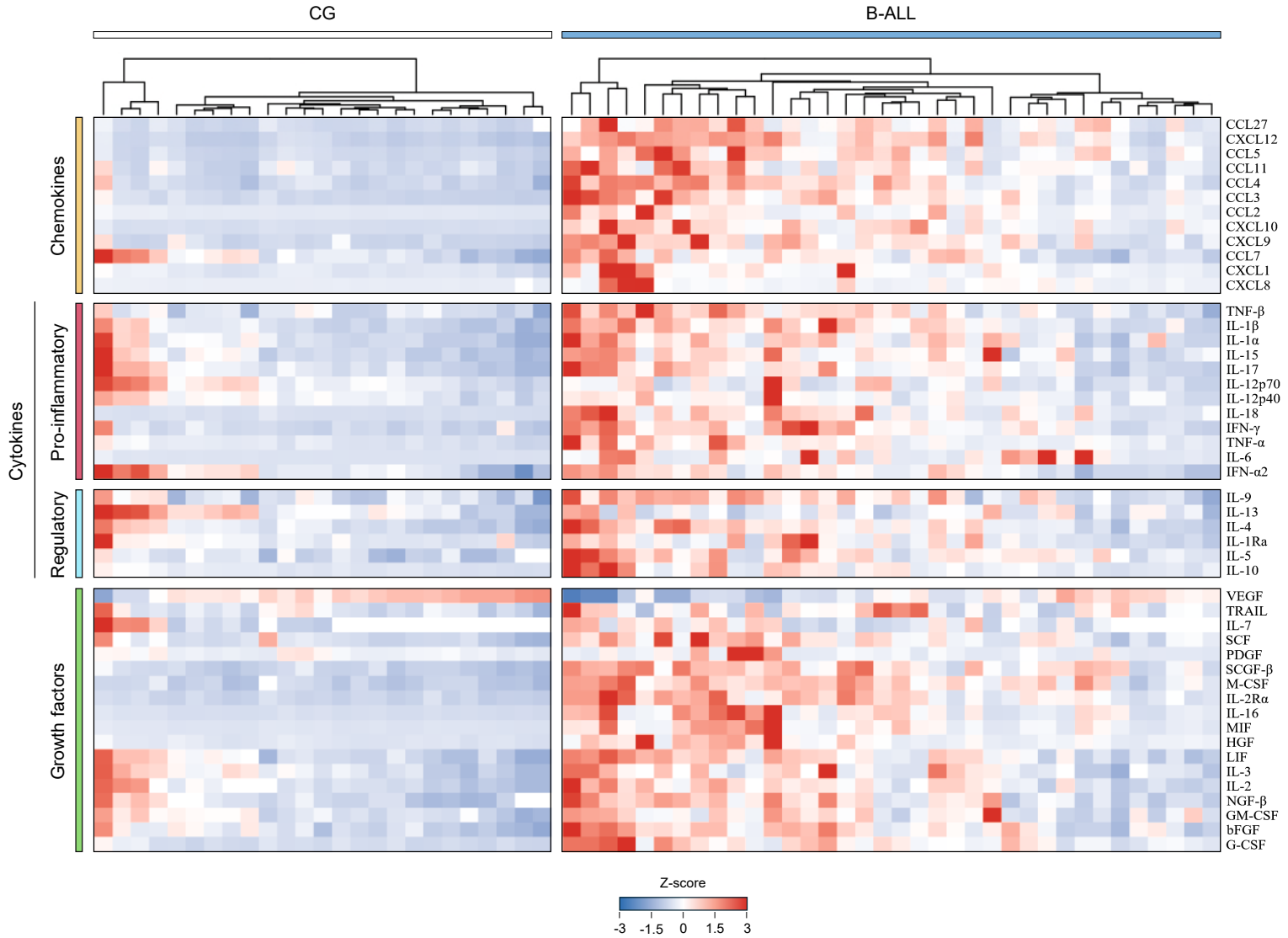
Figure 6. Baseline soluble immune mediator signatures according to clinical outcome in pediatric B-ALL. (A) The signature of soluble immune mediators, including chemokines, pro-inflammatory cytokines, regulatory cytokines, and growth factors, was

787 constructed from the peripheral blood (PB: ◆) and bone marrow (BM: ◆) of B-ALL patients
788 who completed remission chemotherapy (Remission Group - RG), and in the PB (□) and BM
789 (■) of B-ALL patients who died during induction therapy (Deceased Group - DG). Soluble
790 immune mediators were quantified using a multiplex assay, as detailed in the Methods
791 section. Data, originally expressed in picograms per milliliter (pg/mL), were converted into
792 categorical data using the global median as a cut-off point. Signatures are presented as line
793 graphs, with the 50th percentile (red central line: ---) used as a threshold to highlight mediators
794 with increased levels (pink background: □). **(B)** Delta analysis shows the difference in the
795 signature of soluble immune mediators between B-ALL DG and the B-ALL RG for both the
796 PB and BM compartments. Delta values for mediators with a significant difference (Fisher's
797 exact test, $p < 0.05$) are displayed on lollipop charts, with the length of the lollipops
798 representing the magnitude of the difference. **(C)** A Venn diagram highlights the potential
799 biomarkers predicting mortality in pediatric B-ALL patients from PB and BM samples. **(D)**
800 A signature based on mediator classes provides a panoramic view of the profile of
801 chemokines, pro-inflammatory cytokines, regulatory cytokines, and growth factors in B-ALL
802 DG and B-ALL RG. Statistical significance of the proportion of mediator classes was
803 determined using Fisher's exact test, with significant differences denoted by asterisks: ****p
804 < 0.0001.
805
806 **Figure 7. Decision trees and ROC curves of candidate immune mediator panels in**
807 **pediatric B-ALL at diagnosis.** An interpretable decision tree model was constructed to
808 investigate the association between soluble immune mediators and clinical outcomes in
809 pediatric B-ALL patients. The model, based on potential biomarkers predictive of mortality,
810 was developed using the Random Forest algorithm with 500 trees and 20-fold cross-

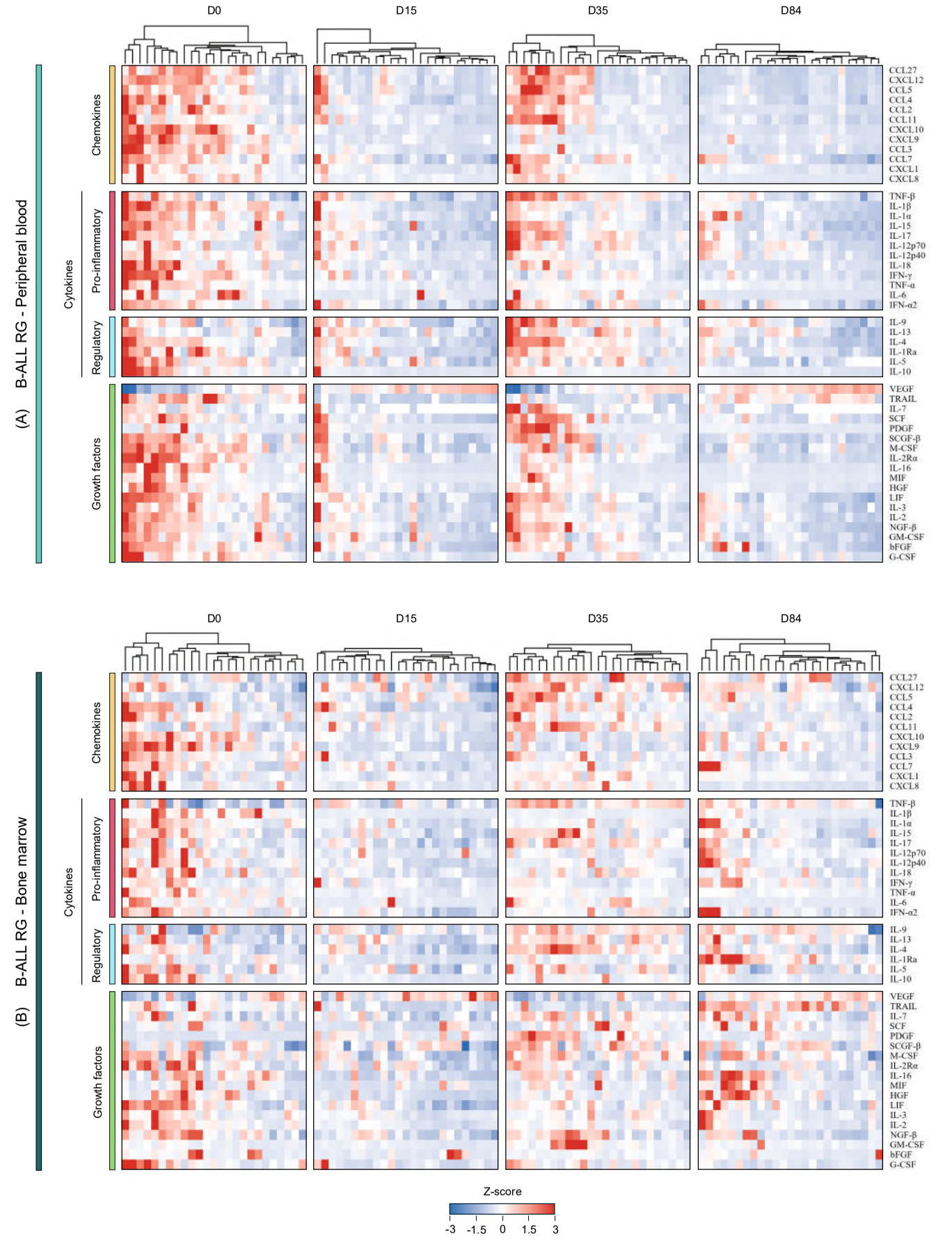
validation. The SMOTE method was employed to correct the class imbalance between the Remission group (RG) and the Deceased group (DG). The ten most relevant variables, based on the Mean Decrease in Gini index, were selected to construct the clinical decision tree using the "rpart" package in R. The tree shows a series of sequential decisions based on the levels of these mediators in peripheral blood and bone marrow samples collected at diagnosis, with each branch leading to a predicted outcome (survival or mortality). Model performance was evaluated using ROC curves, confusion matrices, and metrics such as sensitivity, specificity, balanced accuracy, and F1-score.


Soluble immune mediator profiles in peripheral blood of pediatric B-ALL at diagnosis
Concentration (pg/mL)
CCL2
CCL3
CCL4
CCL5
CCL7
CCL11
CCL27
CXCL1
CXCL8
CXCL9
CXCL10
CXCL12
IFN-α2
IL-1α
IL-1β
IL-6
TNF-α
TNF-β
IL-12p40
IL-12p70
IFN-γ
IL-15
IL-17
IL-18
IL-1Ra
IL-4
IL-5
IL-9
IL-10
IL-13
bFGF
HGF
PDGF
VEGF
NGF-β
TRAIL
IL-3
SCF
SCGF-β
G-CSF
M-CSF
GM-CSF
IL-2Rα
IL-2
IL-7
IL-16
MIF
LIF
CG
B-ALL
Clinical groups

Heatmap of soluble immune mediators in pediatric B-ALL at diagnosis



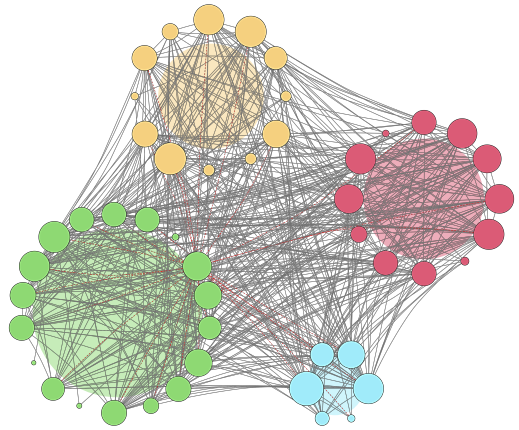
Heatmap of soluble immune mediators in pediatric B-ALL patients during remission chemotherapy



Longitudinal biological networks of soluble immune mediators in pediatric B-ALL

CG = 600 correlations

CG - Peripheral blood



140 (23%) 160 (27%) 78 (13%) 224 (37%)

Order and numbering of soluble immune mediators:

Chemokines

1 - CCL2
2 - CCL3
3 - CCL4
4- CCL5
5 - CCL7
6 - CCL11
7 - CCL27
8 - CXCL1
9 - CXCL8
10 - CXCL9
11 - CXCL10
12 - CXCL12

Pro-inflammatory cytokines

13 - IFN-a2
14 - IL-1α
15 - IL-1ß
16 - IL-6
17 - TNF-α
18 - TNF-ß
19 - IL-12p40
20 - IL-12p70
21 - IFN-γ
22 - IL-15
23 - IL-17
24 - IL-18

Regulatory cytokines

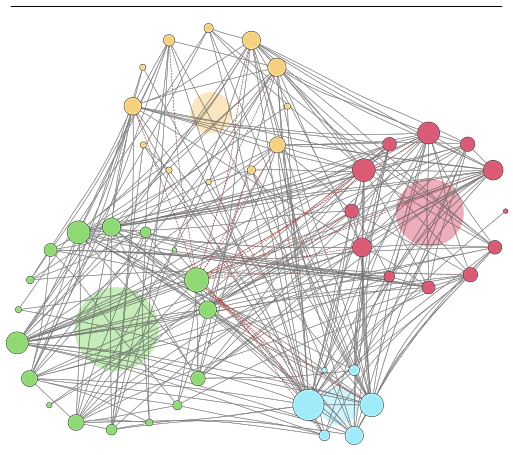
25 - IL-1Ra
26 - IL-4
27 - IL-5
28 - IL-9
29 - IL-10
30 - IL-13

Growth factors

31- bFGF
32 - HGF
33 - PDGF
34 - VEGF
35 - NGF-ß
36 – TRAIL
37 - IL-3
38 – SCF
39 - SCGF-ß
40 - G-CSF
41 - M-CSF
42 - GM-CSF
43 - IL-2Ra
44 - IL-2
45 - IL-7
46 - IL-16
47 - MIF
48 - LIF

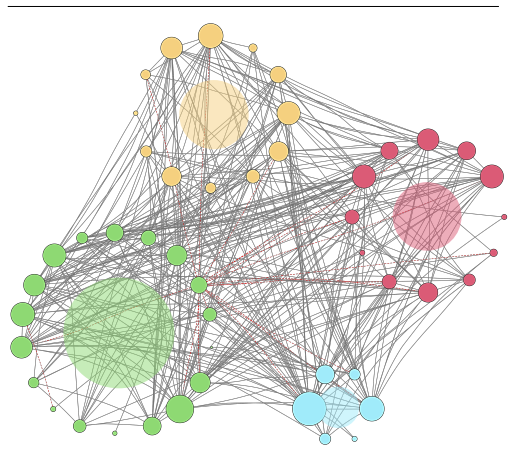
B-ALL RG - Peripheral blood

D0 = 300 correlations



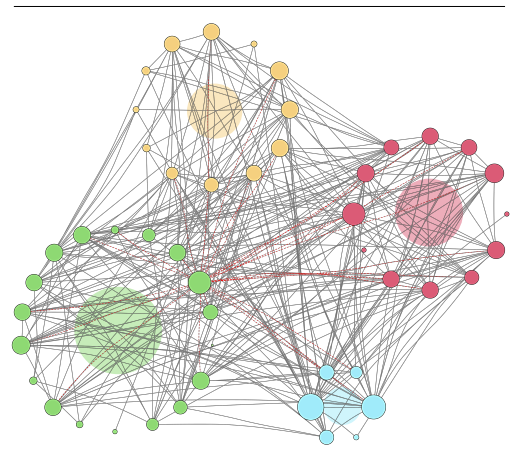
55 (18%) 90 (30%) 51 (17%) 106 (35%)

D15 = 385 correlations



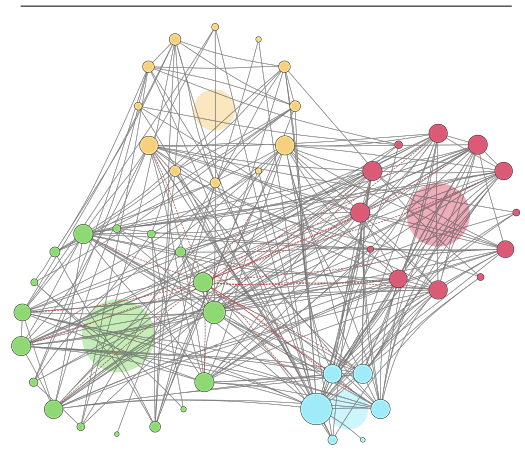
92 (24%) 91 (24%) 55 (14%) 147 (38%)

D35 = 328 correlations



73 (22%) 90 (27%) 50 (15%) 116 (35%)

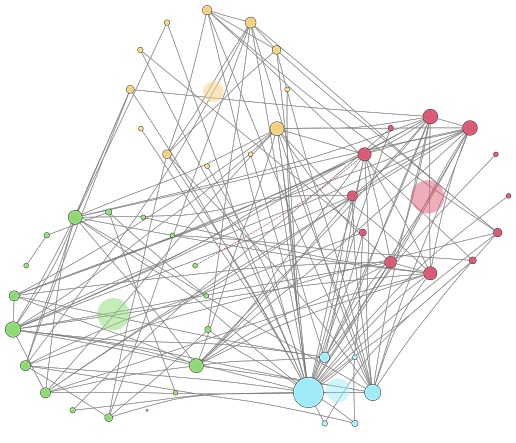
D84 = 286 correlations



55 (19%) 84 (29%) 52 (18%) 97 (34%)

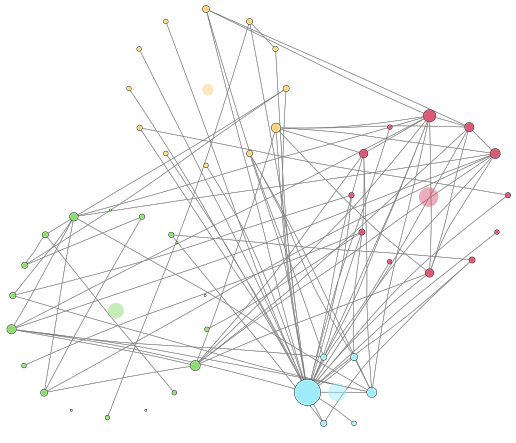
B-ALL RG - Bone marrow

D0 = 146 correlations



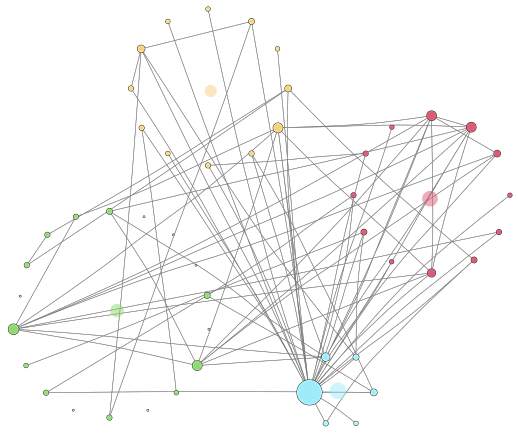
27 (18%) 44 (30%) 32 (22%) 43 (29%)

D15 = 85 correlations



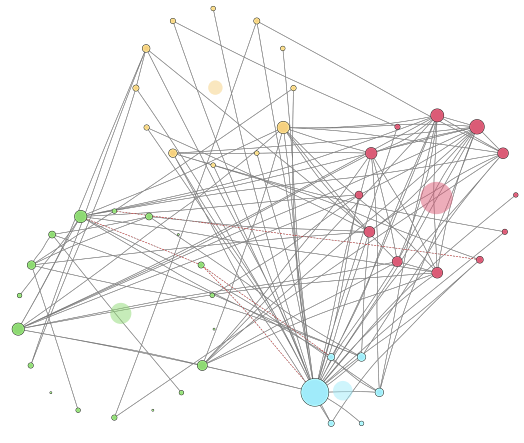
15 (17%) 26 (30%) 24 (28%) 21 (25%)

D35 = 76 correlations



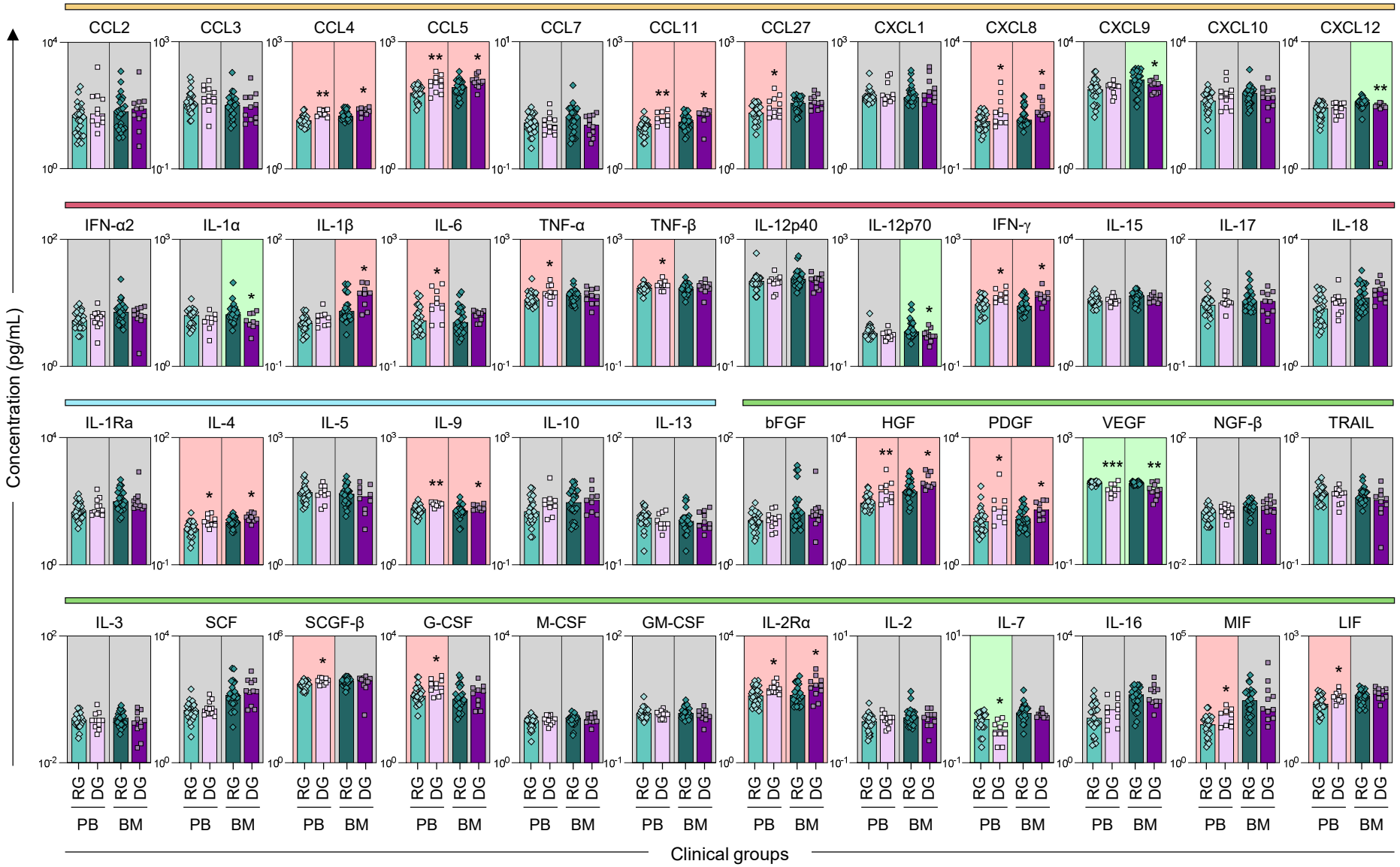
16 (21%) 21 (27%) 22 (29%) 18 (23%)

D84 = 115 correlations



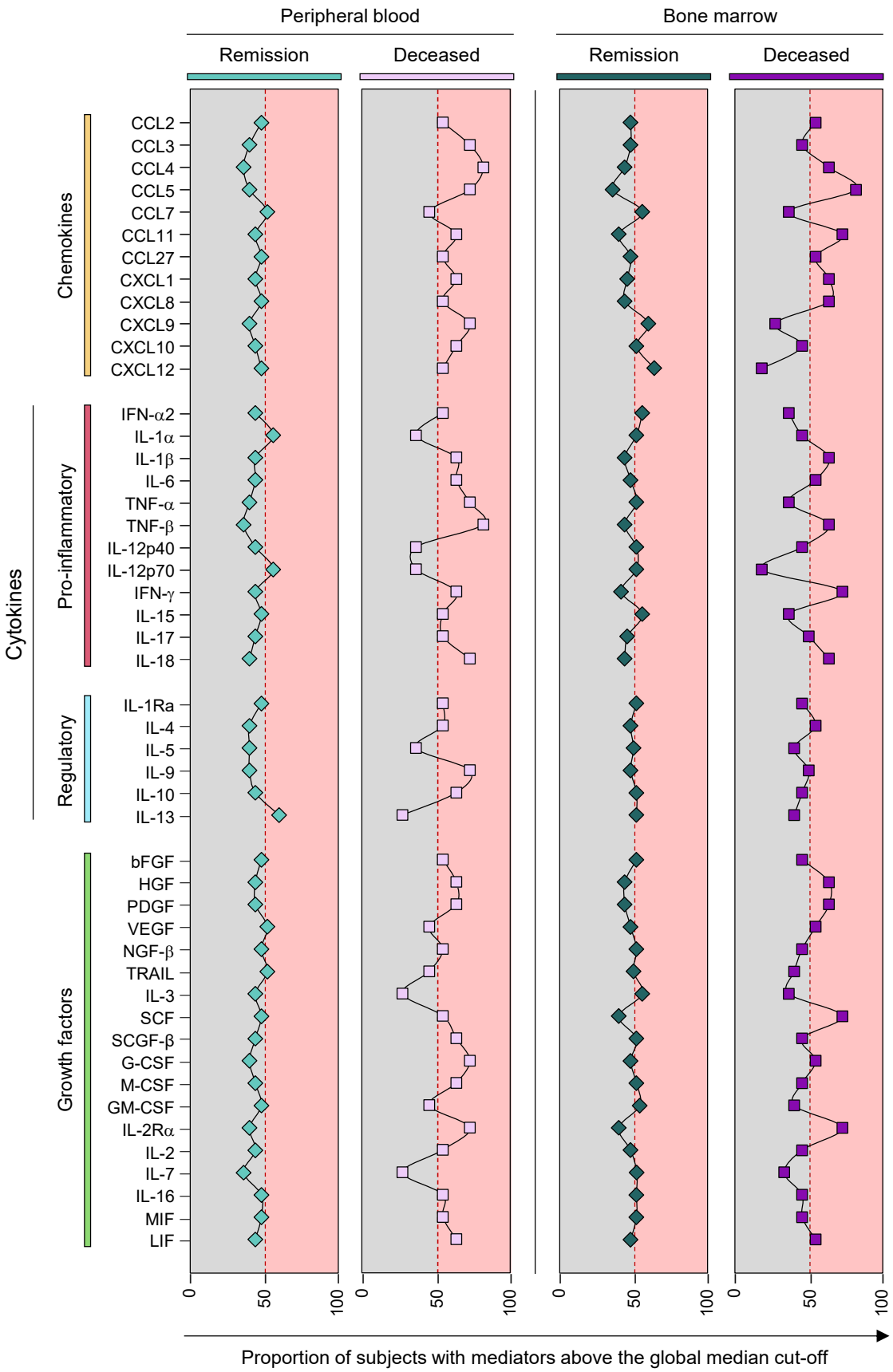
19 (17%) 43 (37%) 26 (22%) 28 (24%)

Baseline immune mediator profiles according to clinical outcome in pediatric B-ALL.

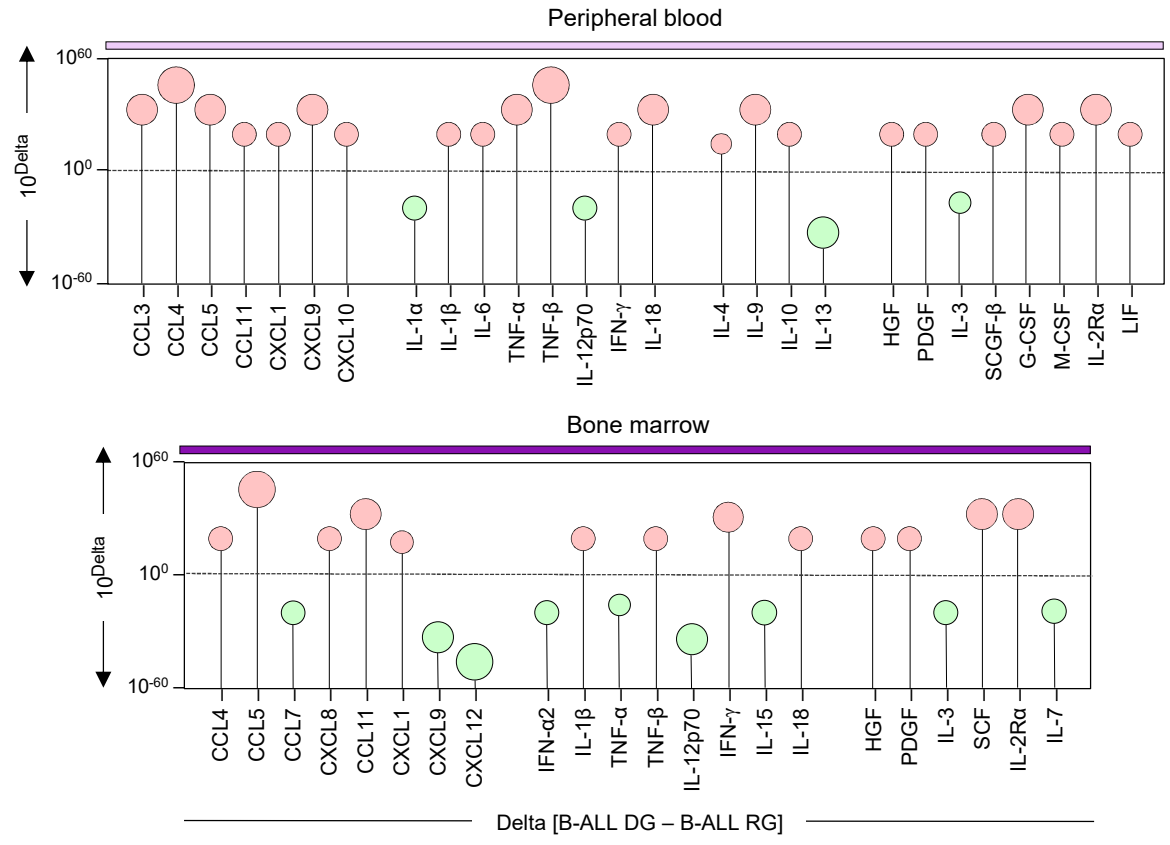


Baseline soluble immune mediator signatures according to clinical outcome in pediatric B-ALL.

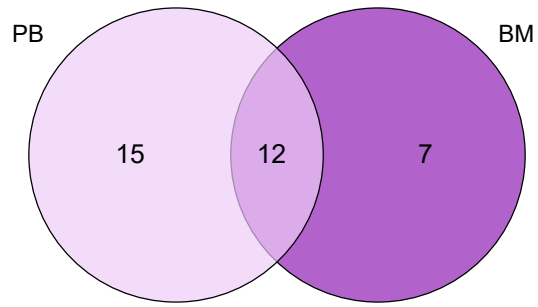
(A) Signature of soluble immune mediators



(B) Delta of potential biomarkers predicting mortality in pediatric B-ALL patients

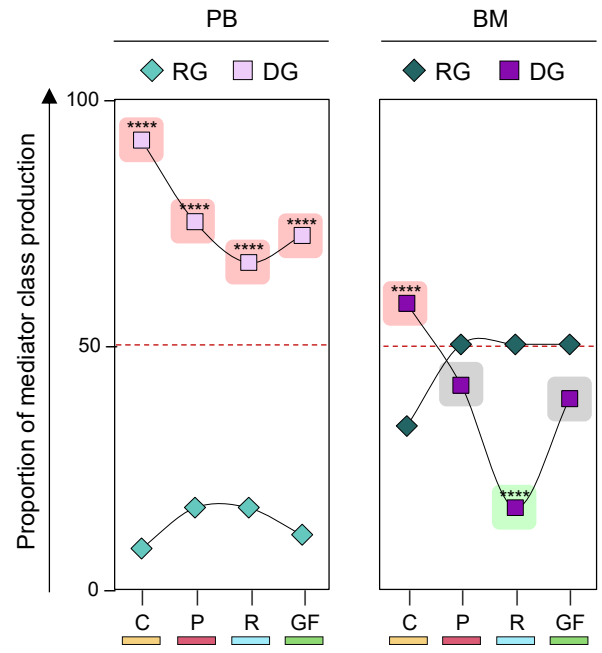


(C) Venn diagram of potential biomarkers



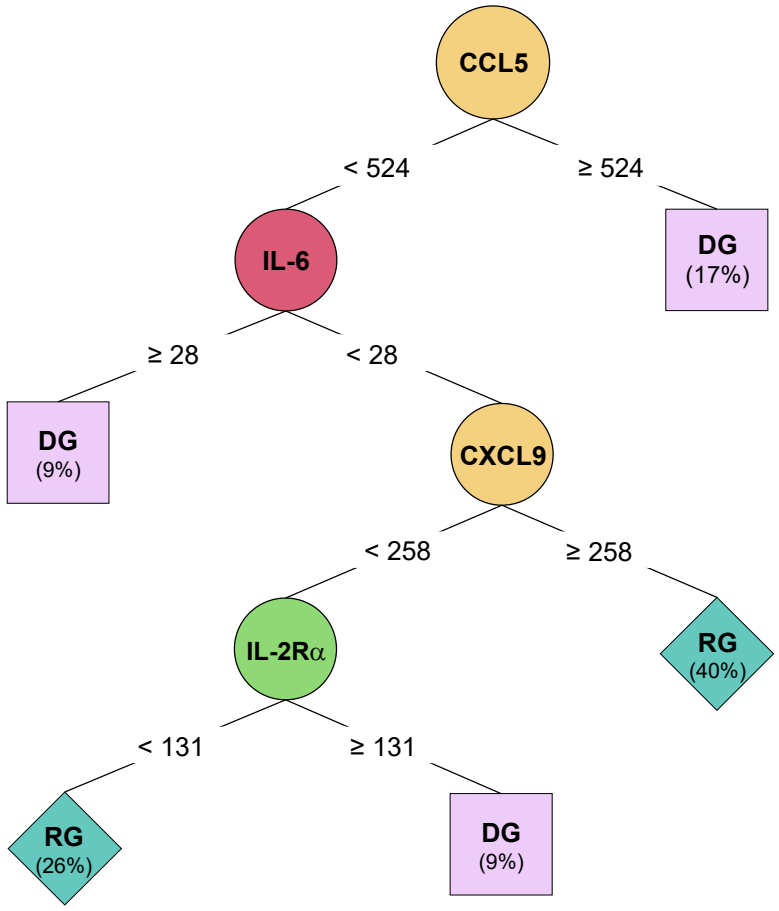
Intersections	Soluble immune mediators
PB = 15	IL-9, IL-13, CXCL10, IL-10, IL-4, CCL3, M-CSF, IL-1α, G-CSF, SCGF-β, IL-6 e LIF
BM = 7	CXCL8, IL-7, SCF, CCL7, IFN-α2, CXCL12 e IL-15
PB & BM = 12	IFN-γ, IL-1β, CXCL1, CXCL9, TNF-β, CCL11, TNF-α, CCL5, IL-18, HGF, CCL4, IL-3, PDGF, IL-12p70 e IL-2Rα

(D) Signature of immune mediator class



Decision trees and ROC curves of candidate immune mediator panels in pediatric B-ALL at diagnosis.

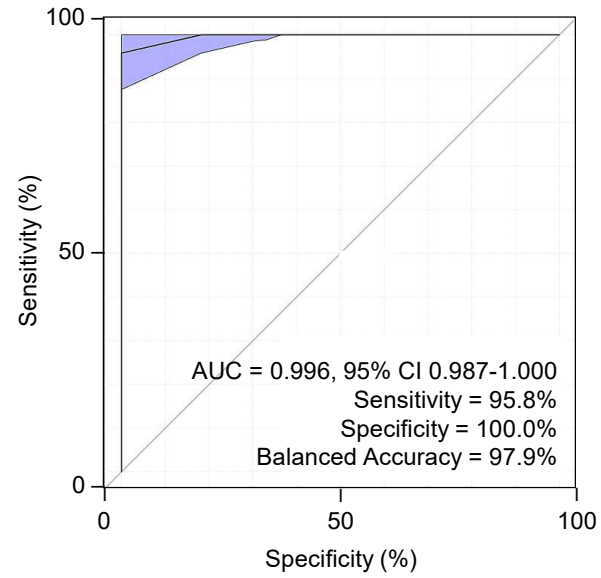
(A) Clinical Decision Tree and ROC Curve based on potential peripheral blood biomarkers



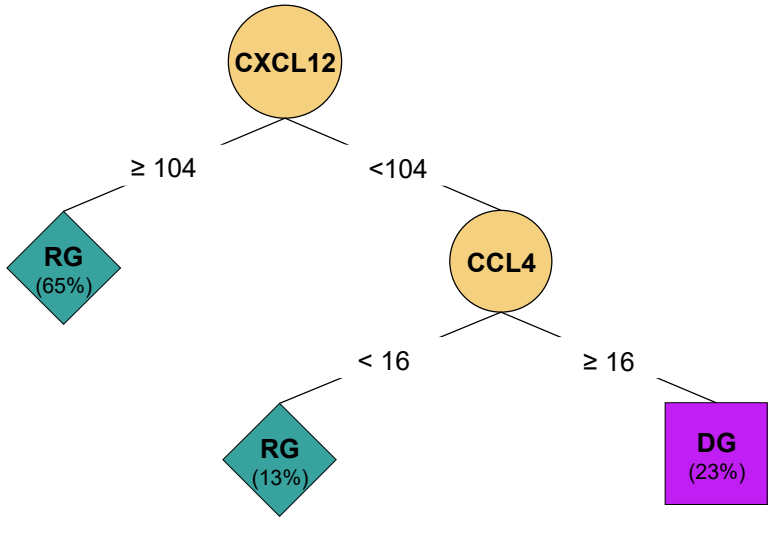
Clinical outcome groups:

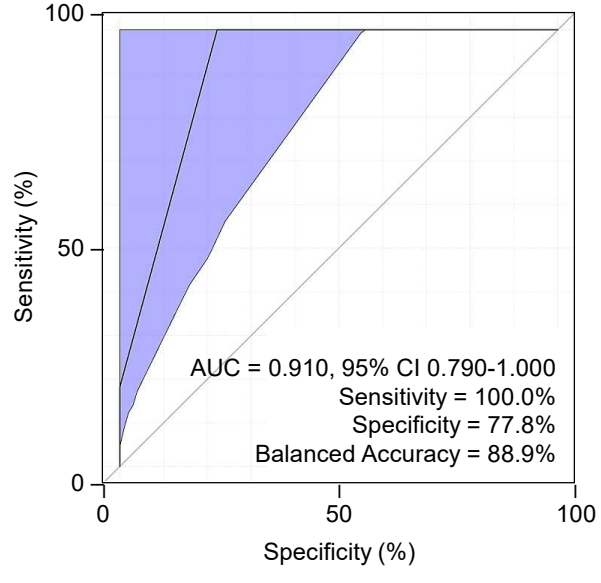
RG = Remission group (completed remission chemotherapy)

DG = Deceased group (died during induction therapy)



(B) Clinical Decision Tree and ROC Curve based on potential bone marrow biomarkers





Supplementary Files

This is a list of supplementary files associated with this preprint. Click to download.

- FigureGraphicalAbstract.pptx
- renamedafa8f.docx